Spring 4-14-2021

Printing Parameter Determination and Characterization of Additively Manufactured Kovar Steel

Will MacGreggor Davidson
University of New Mexico

Will MacGreggor Davidson

Candidate

Mechanical Engineering

Department

This dissertation is approved, and it is acceptable in quality and form for publication:

Approved by the Dissertation Committee:

Peter Vorobieff , Chairperson

Yu-Lin Shen

Dale Cillessen

Printing Parameter Development and Characterization of Additively Manufactured Kovar Steel

By

Will M. Davidson

B.S., Mechanical Engineering, University of New Mexico, December 2020

THESIS

Submitted in Partial Fulfillment of the
Requirements for the Degree of

Master of Science
Mechanical Engineering

The University of New Mexico
Albuquerque, New Mexico

May 2021

DEDICATIONS

For my wife Brittany and my daughter Hope, who enabled this work with their patience, understanding, sacrifice, and hard work of their own. For the rest of our family and friends who supported us in more ways than I can count.

ACKNOWLEDGEMENTS

Thank you to Dr. Deidre Hirschfeld who not only showed me the opportunity to complete this thesis research but enabled it in the first place. Thank you to Dale Cillessen, who guided me through the process and was ever supportive. Thank you to Dr. Kenneth Peterson, Peter Michel, John Lopez, Elizabeth Larkin, Priya Pathare, and Dr. Kevin Strong whose assistance and advice were invaluable.

Printing Parameter Development and Characterization of
Additively Manufactured Kovar Steel

By

Will M. Davidson

B.S., Mechanical Engineering, University of New Mexico, December 2020

M.S., Mechanical Engineering, University of New Mexico, May 2021

Abstract

Kovar (ASTM F15, UNS K94610) steel has many applications across Sandia National Laboratories but is best known within academia and industry for its glass-to-metal and glass-to-ceramic hermetic sealing capabilities. Successful printing parameters for a Renishaw AM400 to additively manufacture artifacts from Kovar steel powder have been determined. The printed test artifacts have been studied for ultimate tensile strength, density, surface roughness, hardness, bulk composition, and impact toughness. Longer throughput measurements such as porosity, coefficient of thermal expansion, and grain structure studies have been established for future delivery to the research team. Yet another delivery from this thesis research is a strategy with which to alter process parameters to achieve more desirable properties was produced. Based on the results of this study a set of design properties, while not yet optimized, is now available.

Table of Contents

List of Figures

List of Equations

List of Tables

Chapter 1 – Introduction

Section 1.1 – Kovar Steel Applications, Market Presence, and the Advantages of A.M.

Kovar steel is an Iron-Nickel-Cobalt alloy (Fe-balance, Co-17%, Ni-29%) used in many products such as x-ray tubes, microwave tubes, high reliability semiconductor packaging, and essentially any application in which a temperature change resistant glass-to-metal seal is required for the last 85 years. Kovar excels in these applications due to its low coefficient of thermal expansion as compared to other metals. This low coefficient of thermal expansion (CTE) is very similar to borosilicate glass and alumina ceramics, and therefore is a good combination to minimize the stress that occurs when two connected materials of dissimilar CTE experience temperature changes. A low CTE also indicates a resistance to thermal shock, a common mode of mechanical failure [1]. Table 1 below shows a comparison of CTE for common materials, though none of these properties are from additively manufactured materials.

Coefficients of Linear Thermal Expansion (0-315˚C)	
Borosilicate Glass	$3 \times 10^{-6}°C^{-1}$ - $6 \times 10^{-6}°C^{-1}$
Alumina Ceramic	$4.5 \times 10^{-6}°C^{-1}$ - $5.5 \times 10^{-6}°C^{-1}$
Kovar Steel	$4.6 \times 10^{-6}°C^{-1}$ - $5.2 \times 10^{-6}°C^{-1}$
17-4PH Stainless Steel	$10.5 \times 10^{-6}°C^{-1}$

Table 1: Coefficients of Linear Thermal Expansion [6]

The global additive manufacturing market size was $8.3 billion in 2019 and is predicted to reach $23.57 billion by 2027 growing at a rate of 14.4% [2]. Additive

manufacturing has many advantages over traditional manufacturing including design features otherwise impossible to produce, manufacturing time, and material cost savings in part coming from the reuse of metal powders. Another advantage of additive manufacturing, while not yet widely used or thoroughly explored, is the ability to tailor a material's physical and mechanical properties to meet specific needs based on the parameter settings with which an artifact is built [3].

Much of the demand for additively manufactured parts comes from industry for three main advantages; design complexity at no extra cost, potential elimination of required tooling, and part consolidation which reduces assembly requirements. All three of these advantages contribute to a reduction in the overall cost to produce a component and are therefore of high interest.

A single example of the positive effect additive manufacturing can have on a particular design can be seen in Figure 2, in which a legacy General Electric aircraft component was replaced by a design 70% lighter [4]. This single design shift to an additively manufactured component increased the efficiency of the aircraft, reduced material waste and labor by eliminating machining, and was fabricated much more quickly than a traditionally manufactured component.

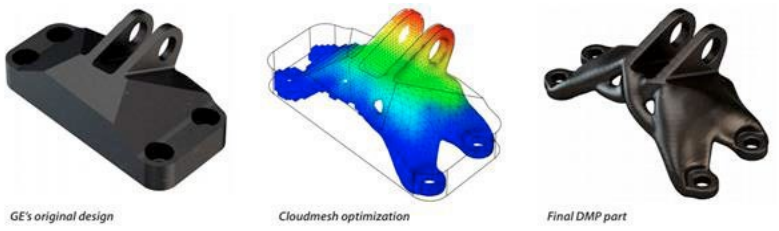

Figure 1: GE Aircraft Engine Bracket Mass Reduction [5]

At the time of this study, there has been no published work concerning the manufacturing of Kovar steel artifacts using an additive manufacturing process. Successfully

combining the applications and need for Kovar components with the advantages of additive manufacturing will contribute to a more efficient and effective product realization cycle.

Section 1.2 – Active Metal Printing Technologies

As of the writing of this thesis, the two leading operations through which additive manufacturing of metals is achieved; Powder Bed Fusion (PBF) and Directed Energy Deposition (DED) based technologies. While both methods have been successful in producing components and have their own applications, PBF methods are most commonly used in industry.

Within PBF technologies, a layer of metal powder is deposited across a surface and then a thermal source, generally a laser or electron beam, selectively melts powder in the desired pattern. These two systems using the different thermal sources are illustrated in Figure 2.

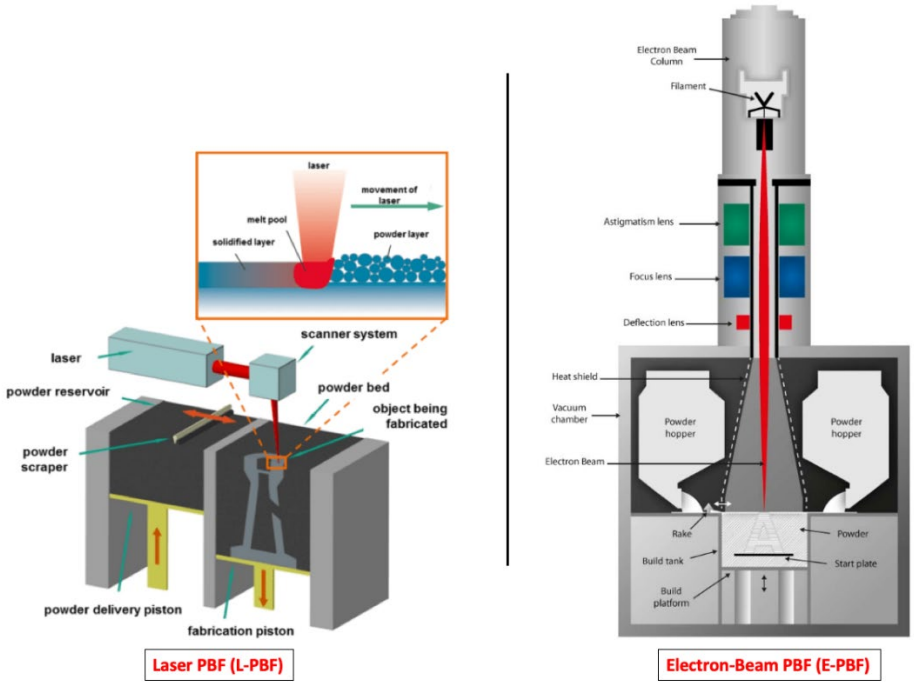

Figure 2: PBF Technologies [9]

PBF methods of additive manufacturing build up a component layer by layer, generally 30 – 70 µm in thickness, until the final dimensions have been achieved. To ensure complete coverage across the build plate excess powder is spread by the wiper, and any that does not remain on the build plate is collected for recycling. PBF methods excel with small details and reach a dimensional accuracy not able to be achieved through DED methods. However, the cost for materials is higher and support structures, seen in Figure 3 below, are often required and need extra post processing such as manual removal.

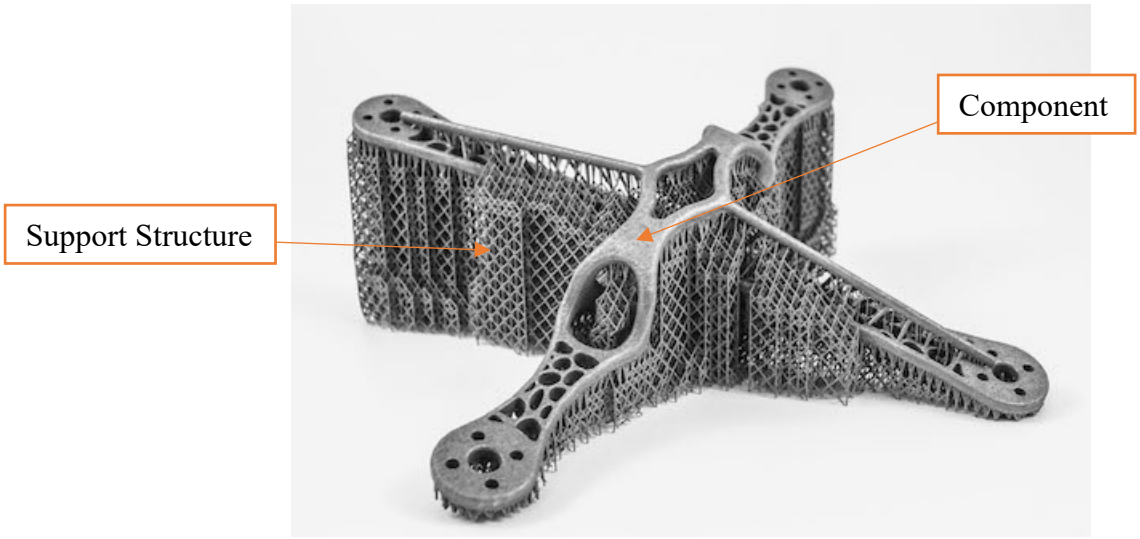

Figure 3: Support Structures on AM Metal Artifact [17]

DED methods include LENS (Laser Engineered Net Shaping), DMD (Direct Metal Deposition), and EBFFF (Electron Beam Free Form Fabrication). All of these methods feed material into a thermal source and deposit the already molten material onto a substrate to build the component. LENS and DMD are two DED methods illustrated below in Figure 4. These systems for deposition are commonly used within a four or five-axis position control system that allows for geometry that is impossible without support structures in PBF. However, DED methods fall significantly short of PBF performance in terms of dimensional accuracy, and components will commonly need to be machined to their final dimensions [6].

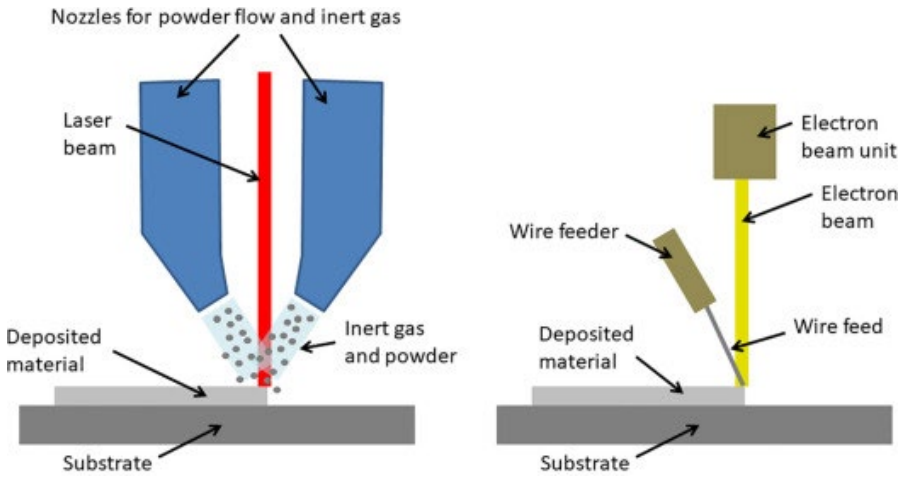

Figure 4: DED Diagram [10]

PBF technology has been chosen for this study in Kovar steel for its as-built dimensional accuracy in producing test specimens adhering to ASTM standards, and for its use and availability at SNL.

Section 1.3 – Renishaw AM400

The Renishaw AM400, shown in Figure 5, is a PBF metal additive manufacturing system that utilizes a 400W laser system with a 70µm beam diameter. The AM400 can fabricate components with a height of up to 28.5 cm, and has a build area of 645 square cm. The printing is completed within the build chamber, while the lower chamber controls the height of the build plate to ensure correct layer thickness and houses the powder collection system.

Figure 5: Renishaw AM400

All components are initiated and built upon a plate of the same or at least a similar alloy as the printed material. The build plate shown in Figure 6 is 25.5 mm thick, however, the thickness of the build plates can vary greatly. Through the PBF process the components are coupled by laser melting to the build plate and wire electrical discharge machining (EDM) is used to cut the artifacts from the plate. Once the printed artifacts are removed the plate is ground flat using a surface grinder, generally losing about 25-50µm of thickness, and then it is ready to be used again.

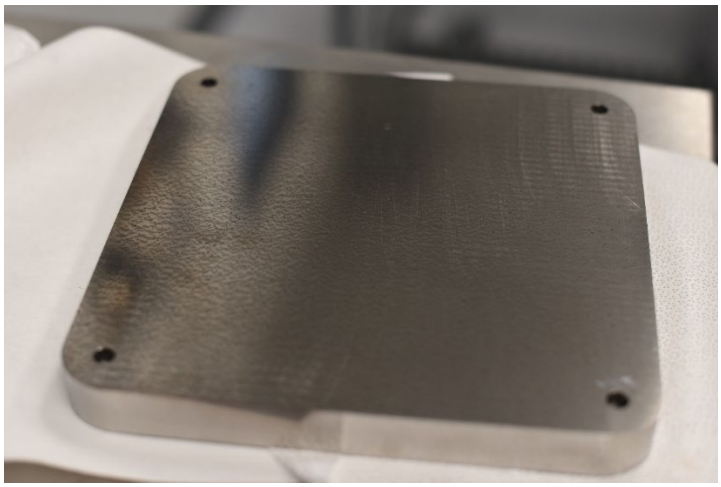

Figure 6: Kovar Steel Build Plate

The printing process is executed within an approximately 4 cubic ft, sealed, Argon-filled chamber. Argon is used for two purposes within this machine: 1) to provide an inert cover gas that replaces air within the build chamber and 2) to remove soot from the powder surface with a constant flow across the build plate. Displacing the air drastically reduces the amount of oxidation occurring within the part impacting physical properties such as density and porosity [7]. Soot removal is critical because soot nanoparticles absorb far more laser energy than the metal powders, and therefore interfere with the melting of the powder leading to voids and other defects within the printed artifact [8]. The effect of the Argon flow (from right to left) on soot removal can be seen in Figure 7, in which there are far more particles exiting the melt pool to the left rather than to the right. The forced Argon flow and a filter element are both part of the system that removes the soot from the build area. The soot is captured in the filter prior to the consumed Argon being released to atmosphere and residual soot is often left along the left side of the build chamber.

Figure 7: Evidence of the Effect of Argon Flow

The direction of the flow also influences the order in which printed artifacts have their next layer melted. The AM400 melts the leftmost components first, and then moves to the right across the plate. In Figure 8 this left to right approach of melting artifact layers across the build plate is shown.

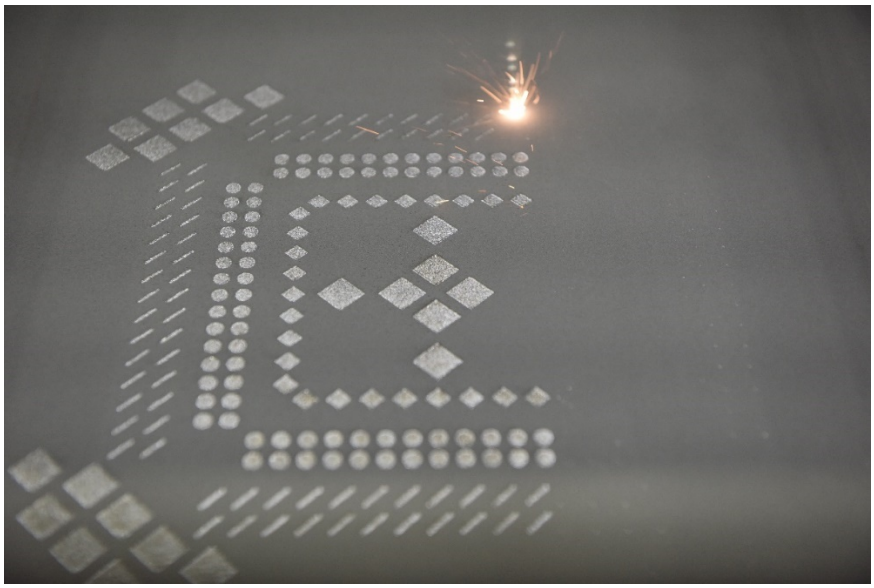

Figure 8: Left to Right Artifact Layer Melting

As the components are built, a layer of powder covers the entire build plate, so when the process is complete the volume of powder on the plate is equal to the area of the plate multiplied by the height of the print. Therefore, there is generally a large amount of excess powder that needs to be removed as shown Figure 9 below. This powder is removed from the build chamber by brushing it into the excess powder collection system built within the Renishaw AM400.

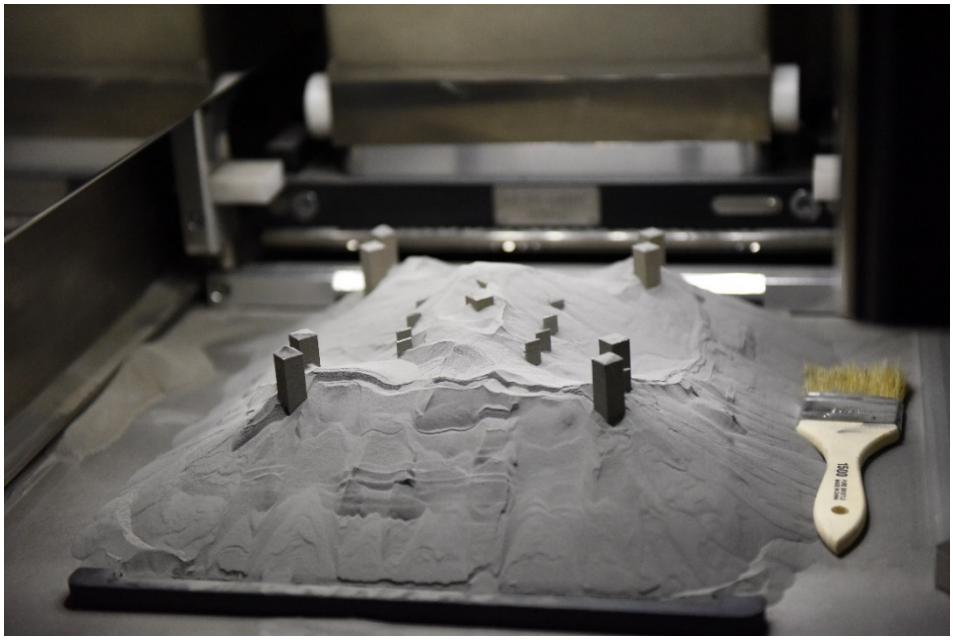

Figure 9: Build Plate with Excess Powder

The excess powder that is collected throughout the build process, and especially once it has been completed, can be reused. However, it must undergo a sieving process before it can be used again to make artifacts. The powder is put through an Argon flooded sieve to remove any oxidized particles and soot that have a larger diameter than the original metal powder, which have been shown to contribute to defects in printed components if present [7]. The sieving process allows for much of the powder to be reused, further cutting waste and cost.

Figure 10: Powder Sieve

Section 1.4 – Need for Study

As stated in Section 1.1, Kovar has many applications across products we use every day, as well as a heavy presence in the research community and at Sandia National Labs. These needs have never been addressed with the design freedom additive manufacturing brings. Determining successful printing parameters for Kovar steel allows for greater speed in

prototyping and production at a reduced cost with the design advantages additive manufacturing allows, with the desired mechanical performance.

Section 1.5 – Experimental Plan

Due to the fact that no previous research has been published on successful printing parameters of Kovar steel, the effects of three parameters were chosen for study; 1) laser power, 2) laser scan speed, and 3) border laser rescan effects. When border laser rescanning is enabled, each layer of the artifact being printed will have the borders melted a second time after the cross-sectional area has been melted. This is typically recommended solely as a cosmetic feature enhancing the surface finish.

The first attempted print used Renishaw recommended general 316L stainless-steel printing parameters and the entire study was completed with completely virgin powder to reduce outside effects on test artifact performance, and absolutely no post processing was performed on the samples. These parameters were chosen for our first attempt at Kovar because laser welding studies have shown that it has similar energy input requirements as 316L stainless steel [12]. For the determination of the effects of laser power and scan speed with a 10% increase and decrease all other parameters were kept consistent. The produced test artifacts were then compared to those produced under the general 316L stainless-steel parameters. For the border laser rescan effect determination, test artifacts were printed under the general stainless-steel parameters, but with the border laser rescans activated. Overall, six sets of test artifacts were printed under different parameter settings as shown in Table 2.

Print Parameter Sets				
Parameter Set	Laser Power	Scan Speed	Borders	Layer Thickness
1 – 316L Settings	200W	90 mm/s	Off	50µm
2 – 316L SS, Borders	200W	90 mm/s	On	50µm
3 – Power Up	220W	90 mm/s	Off	50µm
4 – Power Down	180W	90 mm/s	Off	50µm
5 – Scan Speed Up	200W	99 mm/s	Off	50µm
6 – Scan Speed Down	200W	81 mm/s	Off	50µm

Table 2: Print Parameter Sets

The approach to varying the laser parameters is straightforward; consisting of a ten percent increase or decrease in either laser scan speed or laser power. Varying laser scan speed and laser power directly impacts the amount of energy to which the powder is exposed and has impacts on the final mechanical properties, such as density, of a printed metal [3]. The only difference between parameter sets one and two is that parameter set two has border laser re-scans enabled. No other parameter sets will have border laser rescans enabled.

The printed test artifacts included Charpy Impact bars, CTE bars, both flat and round tensile samples, and density cubes. Position across the build plate has been shown to have slight effects on the printed artifacts, so the artifacts were evenly distributed across the build plate by parameter set. Their position was determined with respect to the center of the build plate, where the laser is most in focus, and therefore has the smallest beam diameter and delivers the greatest energy density to the target. To be able to accurately and reasonably compare two samples of separate parameters and even builds, the artifact sets were placed

such that they were built at the same distance from the center of the plate. The summary of the test artifacts printed per parameter set is illustrated in Table 3.

Test Artifacts per Parameter Set		
Sample Type	Number of Samples	Properties Intended to be Captured
Charpy Bars	5	Impact Toughness, Surface Roughness
CTE Bars	3	Coefficient of Thermal Expansion
Density Cubes	5	Density
Flat Tensile Samples	30	Yield Strength, Ultimate Tensile Strength
Round Tensile Samples	30	Yield Strength, Ultimate Tensile Strength, Poisson's Ratio, Young's Modulus
CT Coupons	1	Bulk Composition, Rockwell B Hardness, Porosity

Table 3: Test Artifacts per Parameter Set

The parameter set which produces the best performing test artifacts will be used to produce a set of physical design properties to allow intentional design with additively manufactured Kovar steel.

The third and final build plate of this initial Kovar steel study is shown in Figure 11 below, and each of the test artifacts present have been labeled.

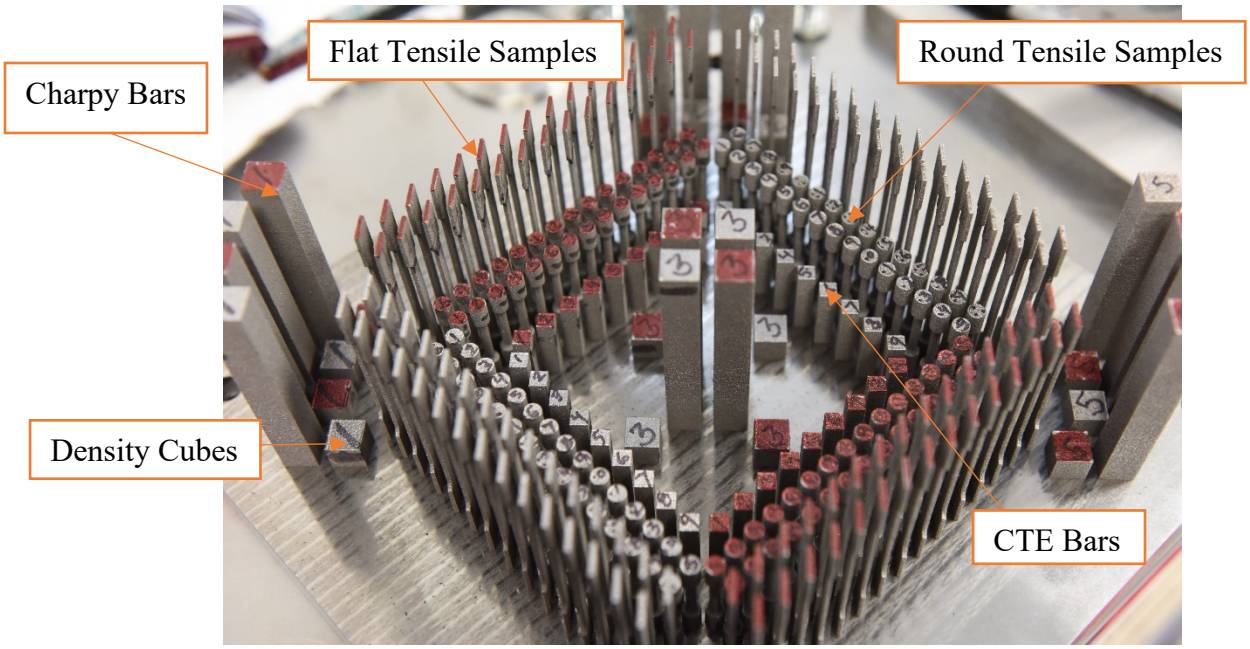

Figure 11: Final Print Build Plate

Chapter 2 – Parameter Validation and Powder Characterization

Section 2.1 – Renishaw AM400 Calibration Impacts

All test artifacts were printed on a Renishaw AM400 that had been calibrated last nearly one year prior to the start of this study. After all the artifacts were printed, the system was re-calibrated over the week of March 1st, 2021. During this calibration the laser power is tested for uniformity across the build plate, the dimensional accuracy of the laser position is tested, and the accuracy of the laser power compared to the set power is determined. The elevator system which controls the build plate position, and therefore the layer height, is cleaned and tested for accuracy. The exact parameters under which the artifacts were printed were determined during this process and were shown to all be within the tolerance specified by Renishaw.

Section 2.2 – Kovar Powder Properties

The Renishaw AM400 system recommends the use of powders in which the average particle size is between 15µm and 45µm. To ensure that the powder used adhered to this recommendation, five separate samples were taken and studied for particle diameter using a scanning electron microscope.

As seen in Table 4, all mean diameter values fall within the 15µm to 45µm recommended range. The samples overall had a mean diameter of 28.57µm, with a distribution curve shown in Figure 12.

Powder Particle Diameters		
	Median Diameter (µm)	Mean Diameter (µm)
Sample 1	25.94	26.93
Sample 2	28.89	29.19
Sample 3	27.40	28.02
Sample 4	29.43	29.55
Sample 5	28.64	29.14

Table 4: Median and Mean Powder Particle Diameters

As seen in Section 1.5, the layer thickness for each parameter set was 50µm, however, the figure below indicates a fraction of the particles present are greater than 50µm. This does not significantly affect the powder distribution across the plate and therefore does not impact the final quality of the artifact.

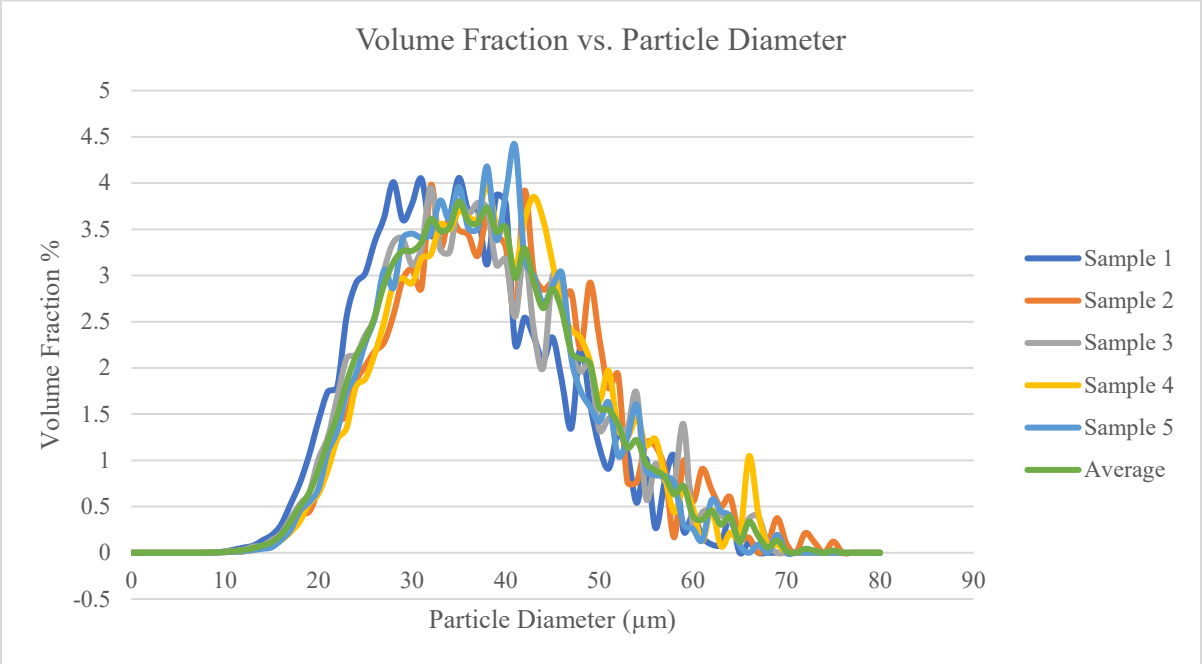

Figure 12: Volume Fraction vs. Particle Diameter of Kovar Steel Powder

An analysis of the powder was also collected at the time of purchase, so that a comparison of the composition of the Kovar steel powder versus the printed Kovar steel artifact could be completed. X-ray powder diffraction (XRD) was used to determine the constituents present within the powder. Within the XRD process the sample of powder is placed upon a rotating fixture between an x-ray tube, and an x-ray detector. When the material is bombarded with the x-rays the atoms within the material are energized and release x-rays characteristic of the elements present [18]. As shown in Figure 13 below, there are spikes on the graph corresponding to the crystallography of Iron, Cobalt, and Nickel. Based on the XRD results, the composition of the powder matches what is expected of Kovar steel.

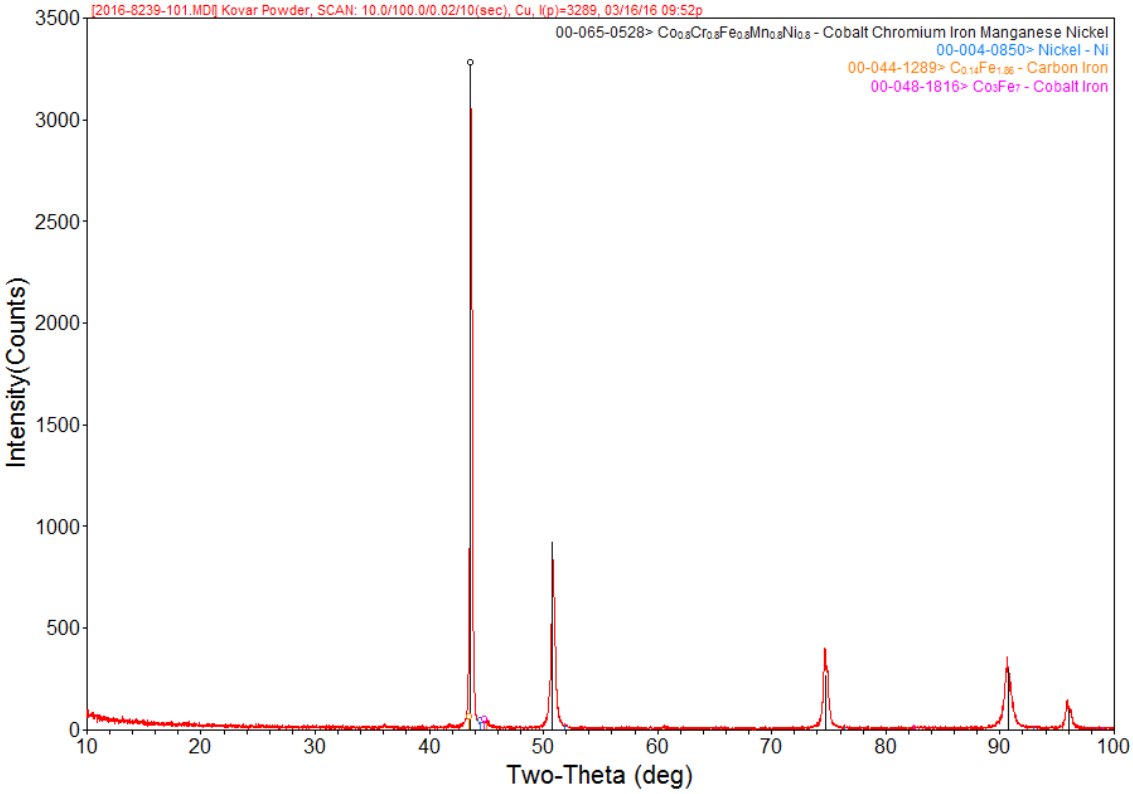

Figure 13: XRD Results for Kovar Powder

Chapter 3 – Experimental Procedure

Section 3.1 – Tensile Samples

Two different types of tensile test samples were designed adhering to ASTM E8/E8M as shown in Figure 14. The flat tensile samples have an active length of 32mm at a 1mm thickness, and an overall length of 64mm. The round samples were designed with an active length of 16mm at a 2.5mm diameter, with an overall length of 35.7mm. These were designed to be overall shorter for the purpose of reducing the overall required build time. Both samples were designed at the dimensions given based on the availability of force sensors. At the time of the study, the only sensor available was a 5kN sensor, and so a theoretical analysis was done to determine an appropriate cross-sectional area. All samples were printed in a vertical orientation, conceptually the weakest orientation in which to print these samples as the force they will experience is perpendicular to the layer pattern. Of course, high-throughput tensile samples both have a lower profile than the ones used here and allow for more samples to be printed on a single build plate, however, at the time of this study there was no access to high-throughput testing.

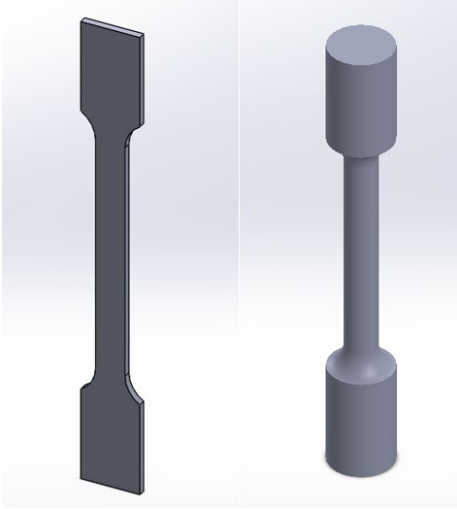

Figure 14: Tensile Sample Models

These samples were designed to be used on an Instron load frame using a 5kN load cell with two different sets clamping jaws, one of which is shown in Figure 15. Unfortunately, at the time of this study an extensometer was not available for use during the tensile testing. The lack of an extensometer means that only stress-based properties such as ultimate tensile strength will be able to be reliably determined. For each parameter setting, except those for “Parameter Set 1 - General 316L Settings”, thirty of each flat and round tensile specimen will be tested to be able to establish a statistical distribution. “Parameter Set 1 - General 316L Settings” has only eighteen total tensile samples, nine of each design, as there were reservations regarding the success of the print. At this point in the study there was only one Kovar steel build plate, so if the plate had been more densely populated and the print failed, EDM time and grinding time would have been drastically increased and result in potentially weeks of lost time.

Figure 15: Instron Tensile Testing

Section 3.2 – Coefficient of Thermal Expansion Bars

The CTE bars were designed to be 5mm square and 25mm long. The samples and tests were performed adhering to ASTM E228 and are shown in Figure 16.

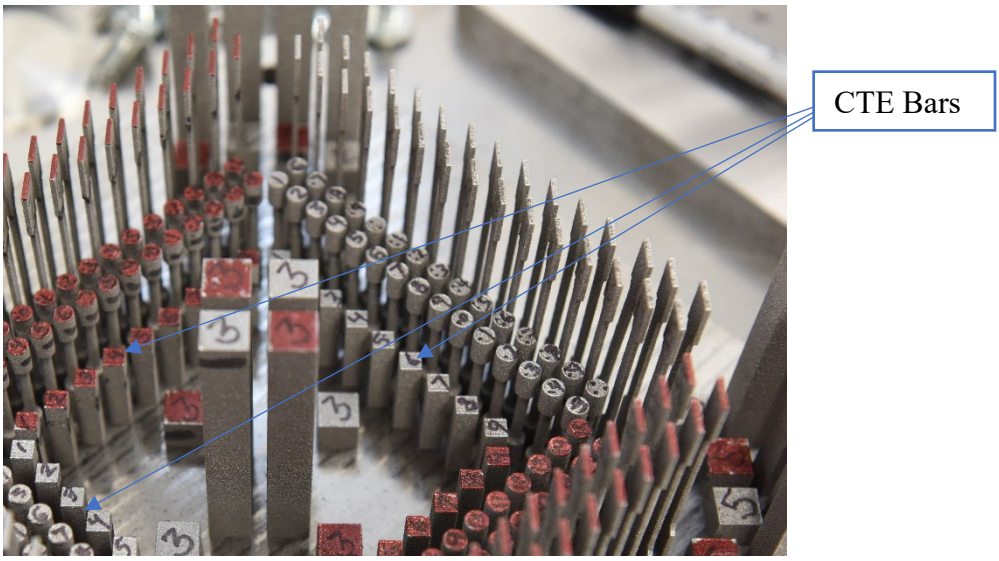

Figure 16: CTE Bars

The tests will be performed under a nitrogen atmosphere and had a temperature range of 0°C to 315°C. Each of the six parameter sets had three bars selected to be tested. CTE was the only property found using these bars. The CTE testing takes approximately twelve hours per sample to complete and were not completed by the writing of this thesis. However, the results will be included in a future publication based on this work. The exact CTE testing machine used for this study, the NETZSCH TMA 402 F1 Hyperion, is shown in Figure 17 below.

Figure 17:CTE Testing Machine

Section 3.3 – Density Cubes

The density cubes, 1 cubic cm, were designed and tested adhering to ASTM B962-17. This process, per the Archimedes Principle, calls for measuring the weight of the cube both dry and submerged in water, three times each using the testing apparatus shown in Figure 18. The density is then found using the Equation 1 in which ρ_a is the density of the artifact ($^{g}/_{cm^3}$), w_d is the weight of the artifact in air (g), w_s is the weight of the artifact submerged (g), and ρ_w is the density of water based on the temperature at the time of testing ($^{g}/_{cm^3}$).

$$\rho_a = \left(\frac{w_d}{w_d - w_s}\right)\rho_w$$

Equation 1: Density Calculation

A surfactant is added to deionized water, in which the cubes are weighed. The purpose of the surfactant is to reduce the surface tension of the water and allow it to wet the rough surfaces produced by the PBF process. The cubes were weighed dry, and after each was weighed it was placed in a beaker of deionized water containing the surfactant. Each cube was submerged for at least ten minutes and agitated to further reduce any surface bubbles that could add error into the calculations. The only material property collected using these test artifacts was density.

Figure 18: Density Testing Kit

Section 3.4 – Charpy Impact Toughness Bars

The Charpy impact test bars were designed and tested adhering to ASTM E23-18. Five samples were printed under each set of parameters with the long axis vertical, which is theoretically the weakest orientation in which to print for this test as the fracture will occur and propagate between layers. This orientation was chosen for two reasons; to reduce the amount of time required to remove the artifacts from the build plate using EDM, and to reduce their build plate footprint so that more artifacts could be printed at the same time.

The Charpy impact test specimen preparation consists of notching the test specimen either through machining or with a rasp to the dimensions described in Figure 19. Once the specimen is prepared, it is broken in two by a pendulum. The pendulum is raised to a known height, so that its potential energy is known. After the sample has been broken, the initial

height of the pendulum, and its maximum height after breaking the sample can be compared to determine the amount of energy absorbed by the sample; the impact toughness.

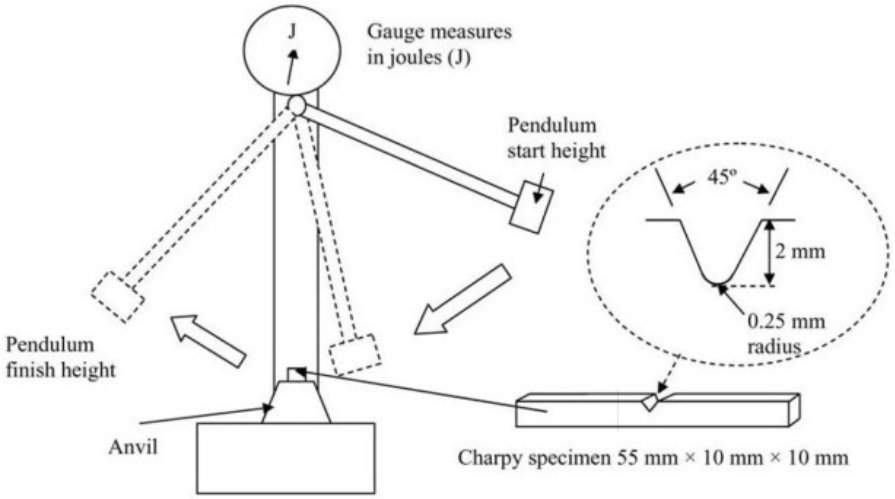

Figure 19: Charpy Impact Test Diagram [11]

The size of the samples, also described in Figure 19, made them ideal to perform other tests as well. The Charpy samples were also used to determine both line and surface roughness per ASTM STP1445 using a Keyence macroscope. Roughness is important information to gather as it has contact mechanics implications on the resistance to wear and friction the final artifact will have. For example, a higher Ra indicates that the surface will have higher coefficients of both static and kinetic friction, and therefore wear more quickly when in an environment where it will experience friction [16]. For the line roughness, the surface of each Charpy bar was measured along thirty-five, evenly spaced, 1.7mm lines. Along these lines both Ra and Rz will be collected.

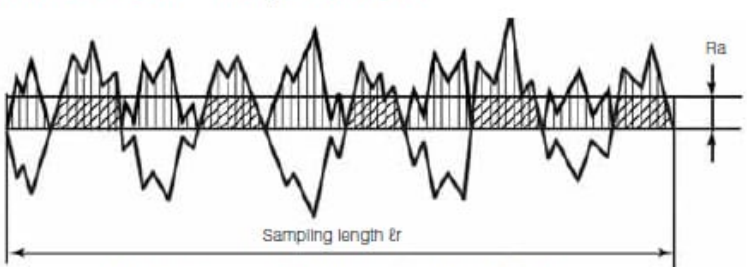

Figure 20: Ra Line Roughness Determination [15]

Ra line roughness is the arithmetic average of surface heights present on a material and is the most commonly used line roughness measurement across the United States [15]. This is visually represented Figure 20 above in which the average of the absolute value of the peak or valley is determined. As previously stated, thirty-five line measurements were taken on each bar and so the average Ra was taken of all measurements. Mathematically, Ra is described in the equation below in which $z(x)$ describes the peaks and valleys present on the material.

$$Ra = \frac{1}{\ell r}\int_0^{\ell r} |z(x)|\, dx$$

Equation 2: Ra Line Roughness Calculation [16]

Rz line roughness, also called the Mean Roughness Depth, is the most commonly used line roughness measurement across Europe [15]. Currently, there are three different accepted methods of Rz line roughness measurement, and it is important to know which method is being used. Within this study we are defining Rz as shown in Figure 21 below.

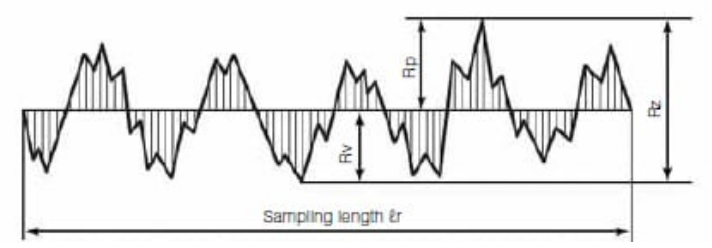

Figure 21: Rz Line Roughness Determination [15]

Within the figure we see that Rz is the sum of Rv, the depth of the deepest valley, and Rp, the height of the greatest peak. As with the Ra calculations, the average Rz of the thirty-five measurements taken will be used and is calculated with the following equation.

$$Rz = \frac{\sum_{i=1}^{n} Rz_i}{n} \text{ in which } Rz_i = Rv + Rp$$

Equation 3: Rz Line Roughness Calculation [16]

Section 3.5 – X-ray Fluorescence and Computed Tomography Coupons

Ten test coupons were printed 25.4mm square by 3.2 mm thick. Each parameter set was used to print two coupons, save "Parameter Set 2 - 316L Borders Enabled". One set was sent for bulk composition using X-ray Fluorescence (XRF), and the others were sent for Computed Tomography (CT) scanning. These coupons were ground flat using a surface grinder to both expose material away from the rough surface and produce a smooth surface on which to perform CT, bulk composition, and Rockwell hardness tests. The grinding process was kept as slow as possible and the artifacts were flooded with coolant throughout to minimize the impact on properties through heating of the surface.

The CT scanning will be used to determine porosity, which is usually increased within additively manufactured materials as compared to traditionally manufactured ones. This testing was performed at Sandia National Laboratories using a WorX Tube x-ray source and a PaxScan 2520DX flat panel detector. The sample was incrementally rotated through 360˚ and mounted at 0˚ to avoid ring artifacts. Ring artifacts are common in CT scans of all steels, including Kovar, because of their tendency to scatter x-rays. At the time of the writing of this thesis the porosity analysis is underway, but initial results have been collected and all results will be present in future publications, and likely part of a future student thesis.

Once CT scanning was complete, but the results not yet analyzed, the same samples were used for Rockwell C hardness testing. Each sample is to be tested at five different locations; each corner and the middle of the sample. Hardness is important to capture as its value quantifies the materials resistance to deformation in all its forms. The Rockwell C Hardness test apparatus is shown in Figure 22.

Figure 22: Wilson Rockwell Hardness Tester

Chapter 4 – Experimental Results

Section 4.1 – Tensile Testing Results

All samples were successfully tested using the Instron system. However, without an extensometer the flat samples produced significantly better curves than the round samples. The most significant effect of conducting these tests without an extensometer was that the elastic portion of the stress/strain curve was not linear, showing that all strain information being gathered lacked accuracy. For this reason, this report will explore the ultimate tensile strength of each parameter set. Another cause of the non-linearity within the elastic zone of the curve for the round samples was the amount of surface area in contact with the jaws of the Instron, which is directly tied to the amount of "settling" required for the jaws to establish a slip-free grip. On the round samples there are four contact points, and due to the geometry of the artifact and the jaws far more "settling" occurs during the test. The Instron jaws used for the round samples are shown below in Figure 23.

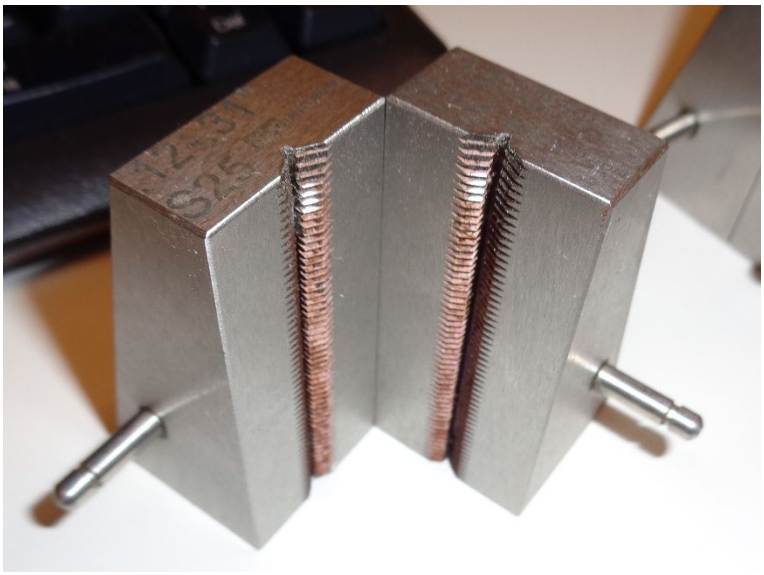

Figure 23: Instron Jaws for Round Tensile Samples

This “settling” indicates that the round samples were experiencing loading and unloading until the slip-free grip was established and could be a direct cause in the wider distribution of ultimate tensile strength results within those samples as seen in Figures 24 and 25 below. As the study moves forward, solutions such as threading each end of the sample for a slip-free grip are being considered. Within the box-and-whisker plots below, the center lines extending out from the box are not error bars, but signify the highest and lowest observed values.

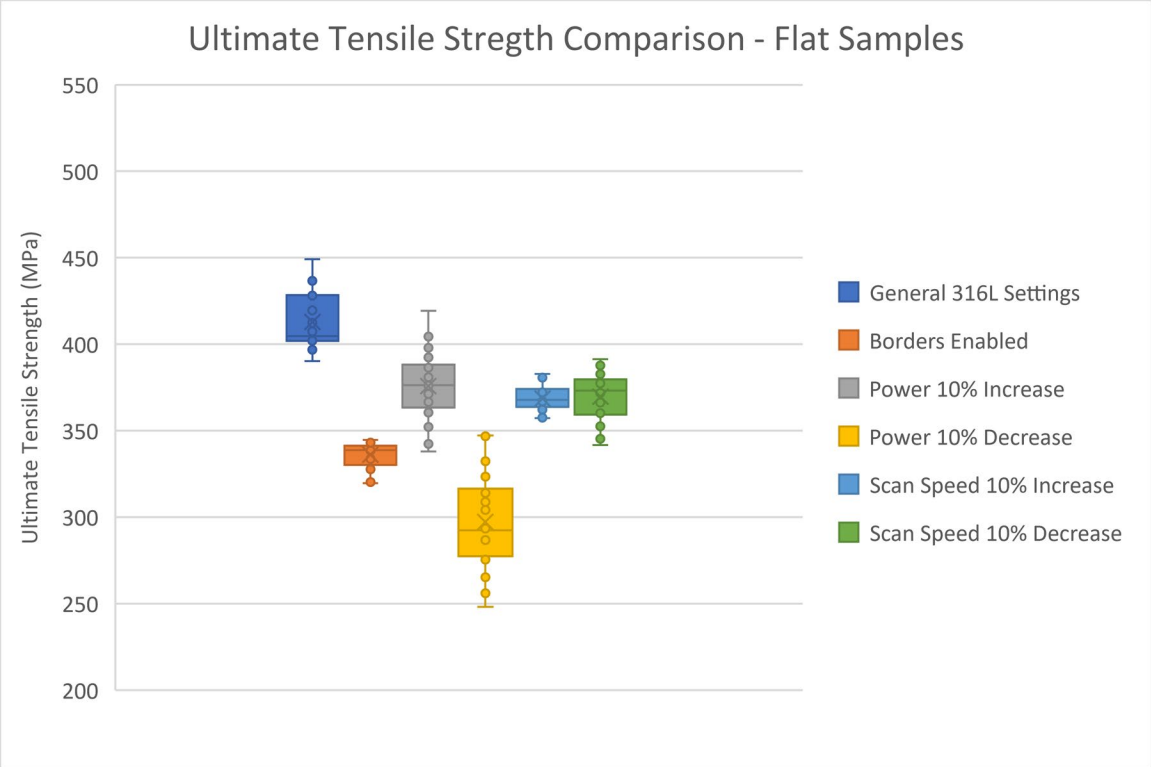

Figure 24: Ultimate Tensile Strength Comparison - Flat Samples

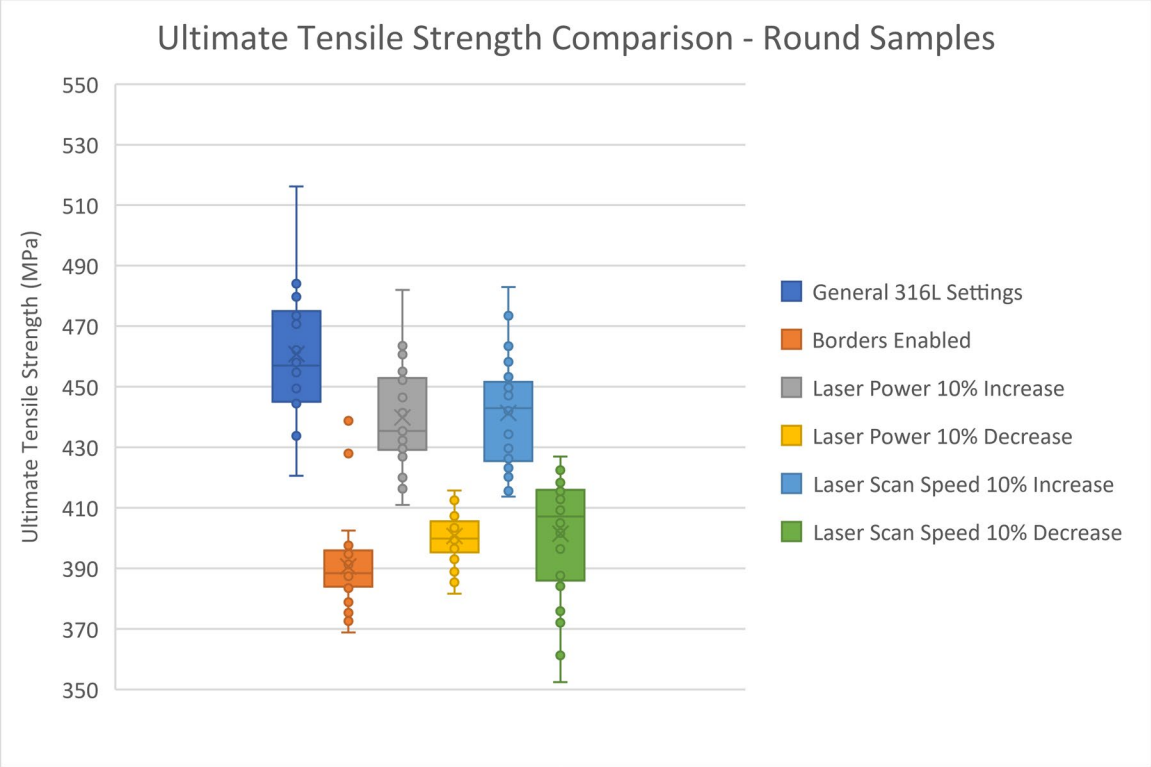

Figure 25: Ultimate Tensile Strength Comparison - Round Samples

Section 4.2 – Density Testing Results

The density testing was performed and completed with no complications and the greatest possible error (GPE) across all testing was only 0.3%. This error was calculated by comparing the results from the three weight measurements both dry and wet. Three density measurements were taken on each cube, and the results can be found in the figures below. As seen in the Figure 26, the difference in density between parameter sets one and two, General 316L Settings and Borders Enabled, is significant.

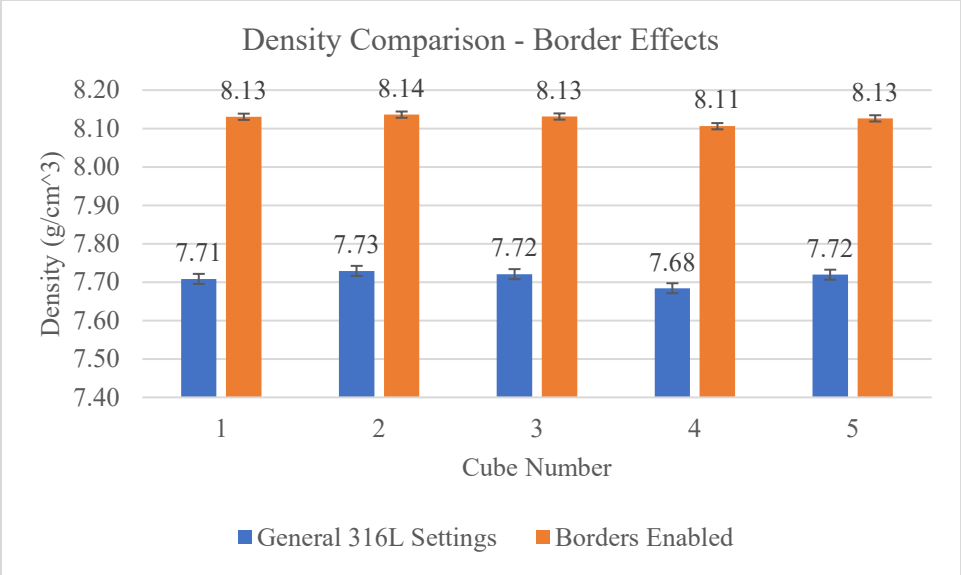

Figure 26: Density of General SS Compared to Border Re-Melting

While some difference is expected, the disparity shown is far greater than expected and so requires further exploration. As part of the build process, the atmosphere within the build chamber is evacuated of air and filled with Argon. The day of the first build, the printer ran into quite a few problems while trying to achieve the Oxygen levels required to start the printing process. After consulting with engineers at SNL who specialize in metal additive manufacturing, this difficult atmosphere replacement has been suspected as the cause, but no specific reason for the disparity has been discovered. Due to the fact that the density cubes printed under "Parameter Set 1 - General 316L" settings could not be used for a reliable comparison, the following parameter sets will be compared to one another.

As seen in Figure 27, there is no correlation present to suggest that either increasing or decreasing the amount of energy, by the amounts explored in this study, significantly impacts the density of the finished parts. Parameter sets two through six all had 96-97% density as compared to traditionally manufactured Kovar steel.

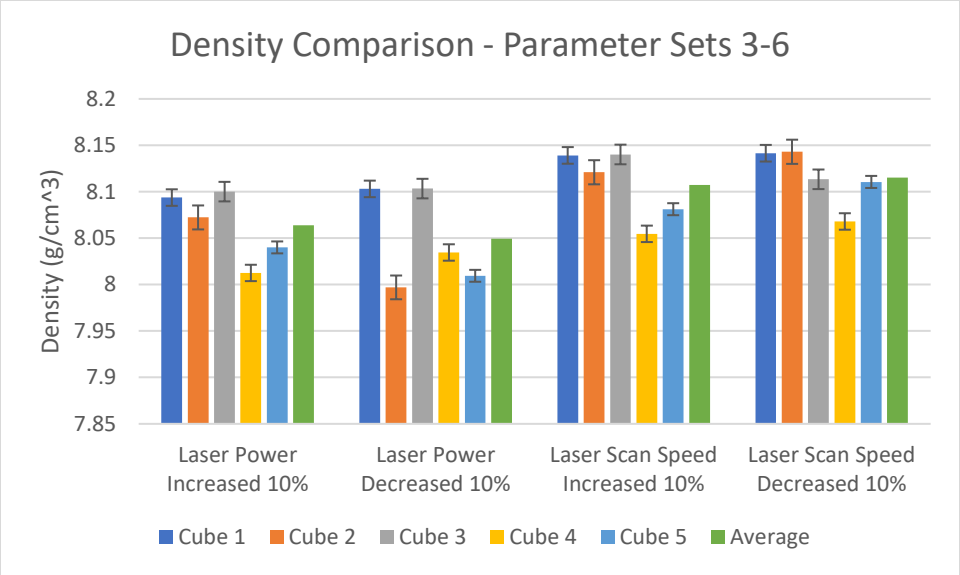

Figure 27: Density Comparison - Laser Power and Scan Speed Affects

Consistent in all but one parameter set, density cube number four had a lower density than the others. One factor contributing to this pattern could be the fact that the position of an artifact on the build plate can impact its properties [3]. A cause of this inconsistency across the build plate in part comes from the laser system itself. The laser is most in focus at the center of the build plate, and as it moves to the edges of the plate it becomes more out of focus. While cubes 1, 2, and 5 were also the same distance from the center of the build plate, a consistent underperformance in that position could indicate a flaw in the optics that is resulting in less power reaching that portion of the plate. This issue will likely be resolved as this work goes forward with much larger sample sizes.

Section 4.3 – Charpy Testing Results

Charpy testing was completed on all 30 samples, save one. Originally the Charpy testing machine was set to deliver 135 Joules to the sample, however, after the first sample of "Parameter Set 2 - Laser Power 10% Increase" managed to stop the pendulum the machine

was set to deliver 325 Joules. Needless to say, some toughness values exceeded expectations. A comparison between “Parameter Set 1 – General 316L Settings” and “Parameter Set 1 – 316L Borders Enabled” is shown below in Figure 28.

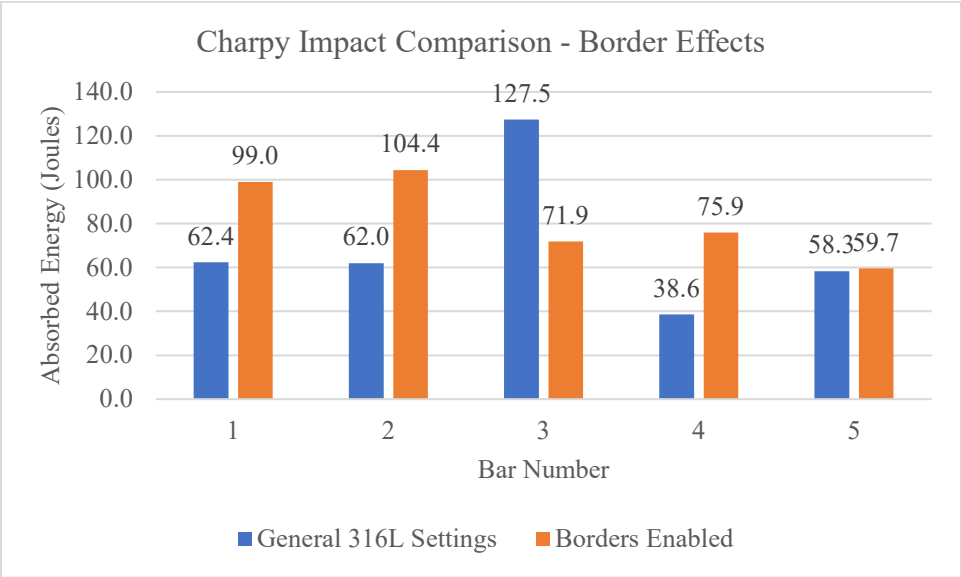

Figure 28: Charpy Impact Comparison - Border Effects

While outliers from the average are common in Charpy impact testing, the results from “Parameter Set 1 - General 316L Stainless Steel” are far more inconsistent than the results from “Parameter Set 2 - 316L with Borders Enabled”. This greater consistency likely comes from the greater surface uniformity of the samples from Parameter Set 2.

Increasing the laser power to 220W (Parameter Set 3) drastically improved the amount of energy produced by the pendulum absorbed by the samples, while decreasing the laser power to 180W (Parameter Set 4) consistently underperformed both of the comparators. This is clearly illustrated in Figure 29.

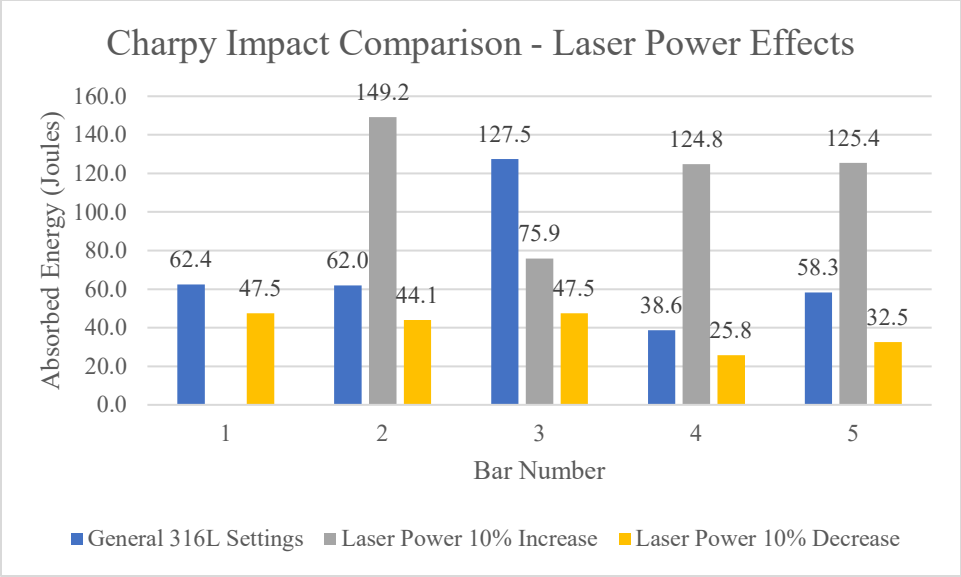

Figure 29: Charpy Impact Comparison - Laser Power Effects

Altering the scan speed with "Parameter Set 5 - Scan Speed 10% Increase" and "Parameter Set 6 - Scan Speed 10% Decrease" did not result in better results than "Parameter Set 1 - General 316L Settings", as shown in Figure 30.

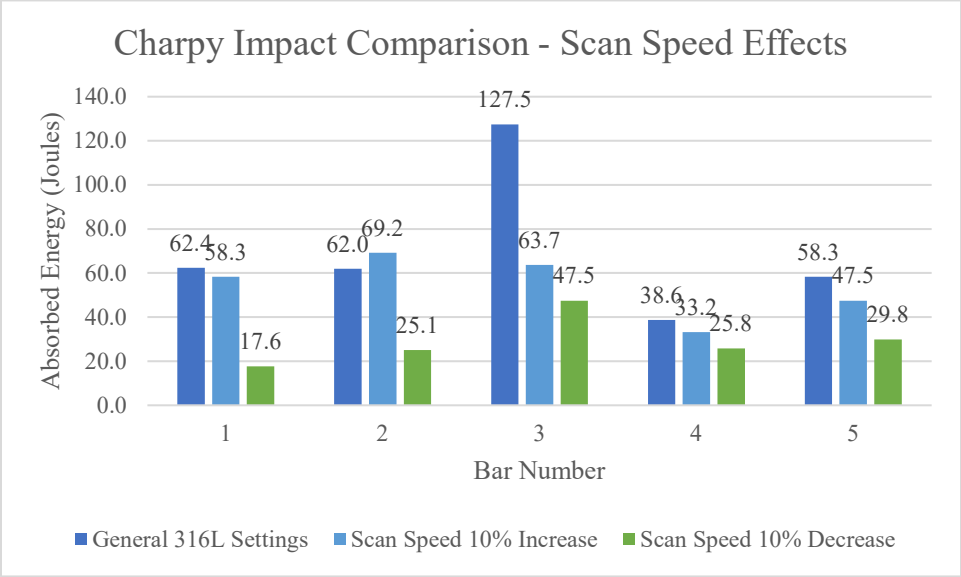

Figure 30: Charpy Impact Comparison - Scan Speed Effects

Based on the Charpy impact testing results, “Parameter Set 3 - Laser Power 10% Increase” had both the greatest amount of energy absorbed, and the most consistent results.

Section 4.4 – Rockwell Hardness C Results

As stated in Section 1.5, each test coupon was measured for hardness at five different locations; approximately 5mm from each corner, and the center of the coupon. In the figures below, a comparison is made between the General 316L settings and the other parameter sets. “Parameter Set 2 – Borders Enabled” was not included for these comparisons, as the measurements are being taken after the surface is ground smooth, removing any effect the border scans would have. A comparison to illustrate the effect of varying laser power is shown in Figure 30. As can be seen, both increasing and decreasing the laser power produced artifacts with a greater hardness, but only by an increase 4.3% for Laser Power Decreased 10% and an increase of 3.8% for Laser Power Increased 10%.

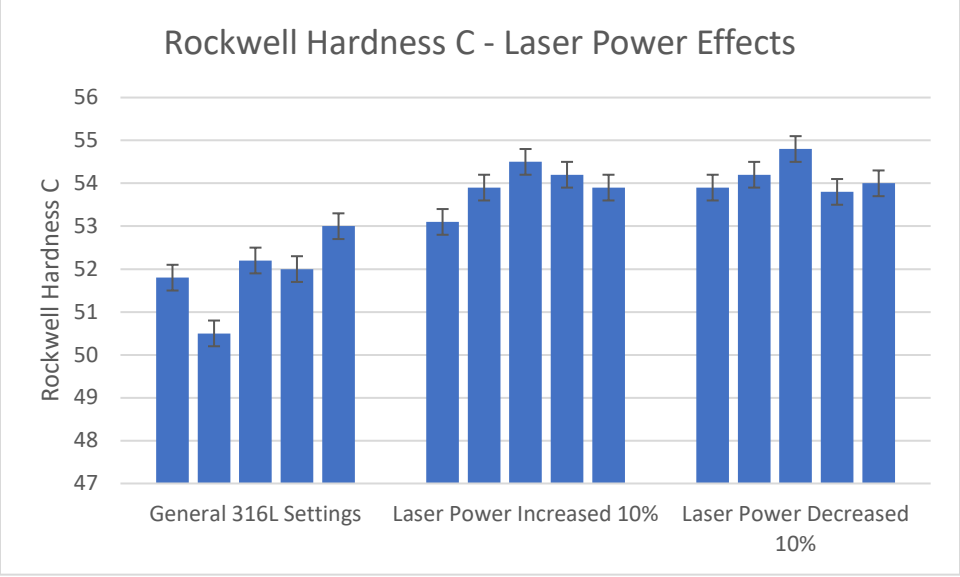

Figure 31: Rockwell Hardness C - Laser Power Effects

The results for the scan speed variation are similar to those of the laser power variation as illustrated in Figure 32.

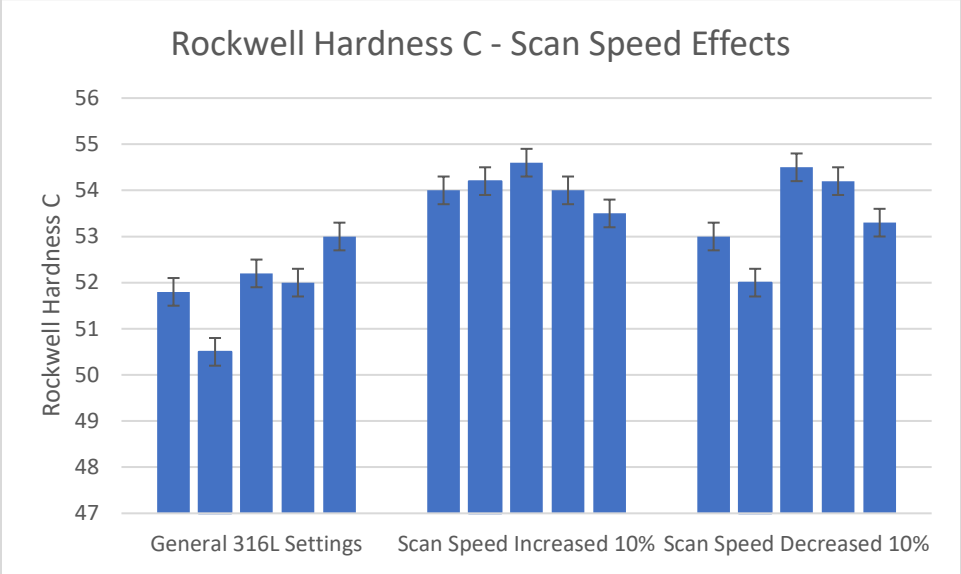

Figure 32: Rockwell Hardness C - Scan Speed Effects

Both setting changes resulted in an increase in average hardness across the artifact, 4.2% increase for "Parameter Set 3 - Scan Speed Increased 10%" and a 2.9% increase for "Parameter Set 4 - Scan Speed Decreased 10%". While decreasing the amount of energy put into the artifact through increasing the scan speed and decreasing the laser power both resulted in higher Rockwell C hardness values than increasing the amount of energy, it is not by a large enough amount to have a certain result. These results indicate that either the parameters were not varied enough to see a clear result, or that the hardness is not very dependent on the energy put into the artifact during the printing process [3].

Section 4.6 – Roughness Results

As stated in Section 3.4, both surface roughness and line roughness measurements were collected. The surface roughness studied an area of 2.7 square mm, and the line

roughness was repeated thirty-five times per sample over a length of 1.7 mm. As seen in the Figure 33, the General 316L Settings performed best in terms of Ra.

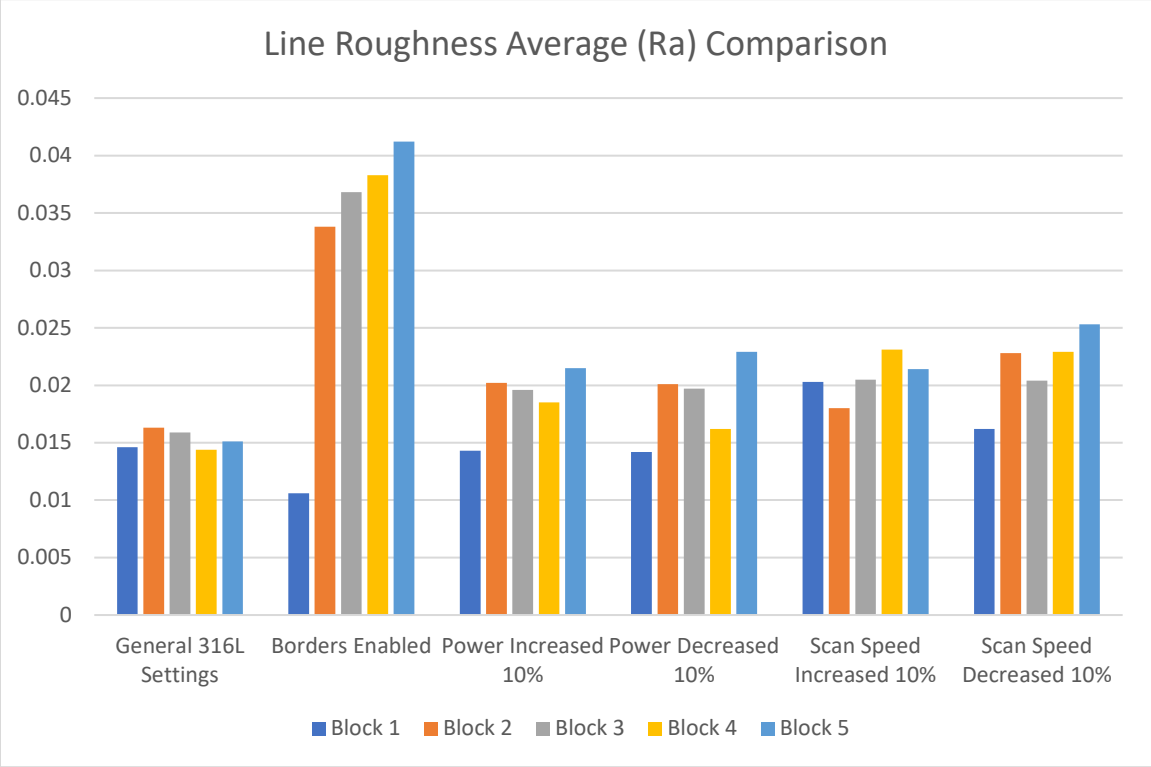

Figure 33: Ra Comparison

When comparing the General 316L Settings results to the Borders Enabled results, the Borders enabled clearly has a significantly higher Ra value. This is of note because the border rescans are meant solely as a cosmetic feature on the printed artifact, and yet of the six parameter sets, the Borders Enabled had nearly twice the Ra value of the others.

Consistent with the Ra results, the Rz results follow the same trend as seen in Figure 33. Again, the Borders Enabled parameter set had the largest Rz values, meaning it had the greatest peaks and the deepest valleys along its surface. Also consistent with the Ra results, “Parameter Set 1 - General 316L Setting”s had on average the best results.

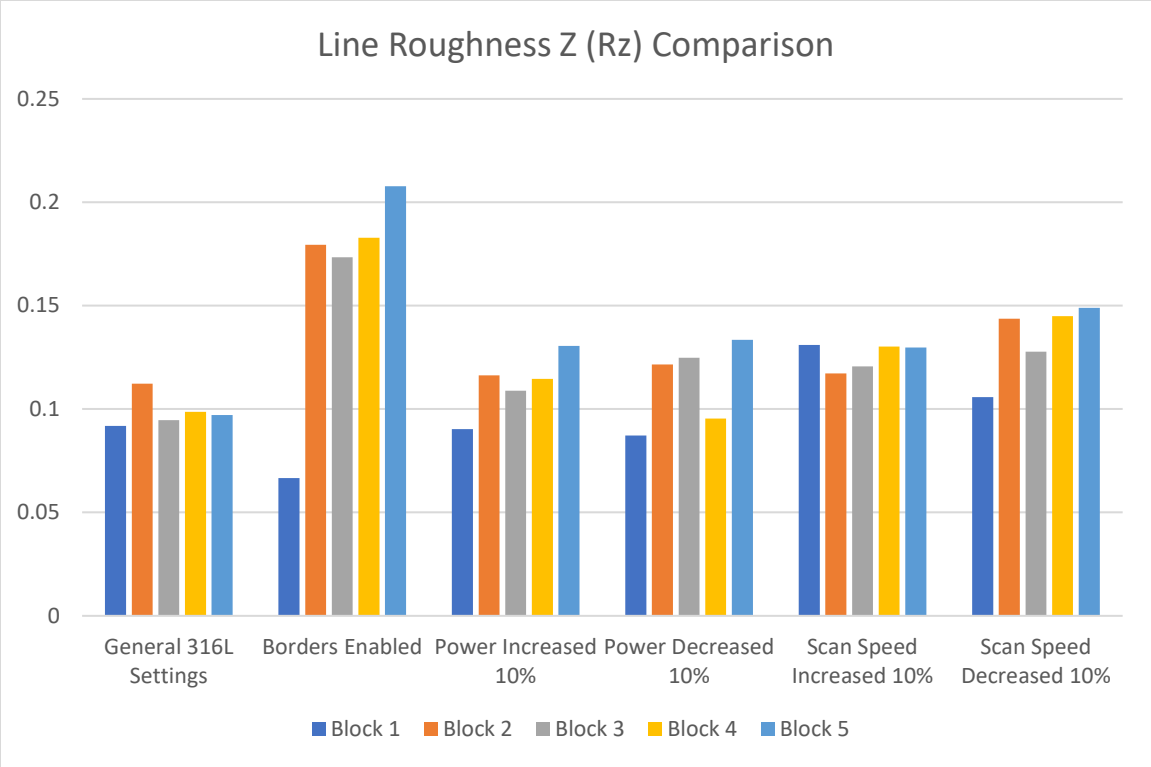

Figure 34: Rz Comparison

Figures 34 and 35 below illustrate the Sa and Sz results for the six different parameter sets, and as expected based on the Ra and Rz, "Parameter Set 1 – General 316L Settings" outperformed all other parameter sets in terms of roughness, both on average and with consistency across the different Charpy bars.

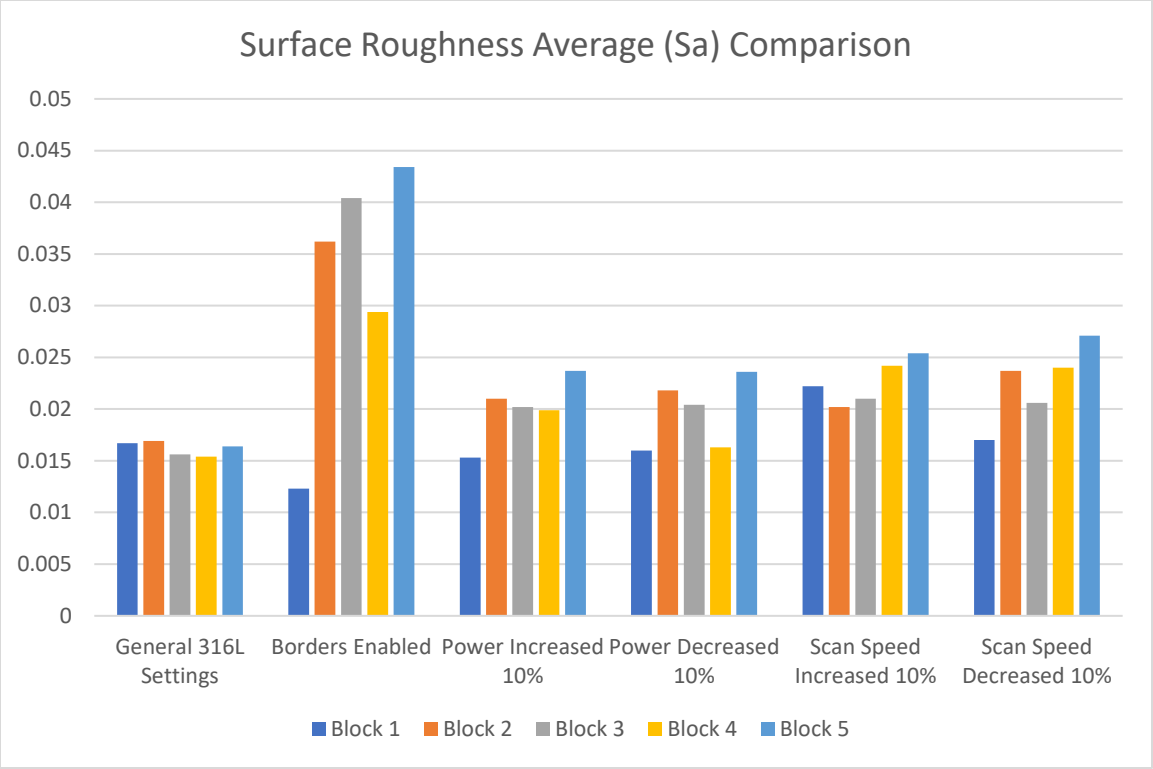

Figure 35: Sa Comparison

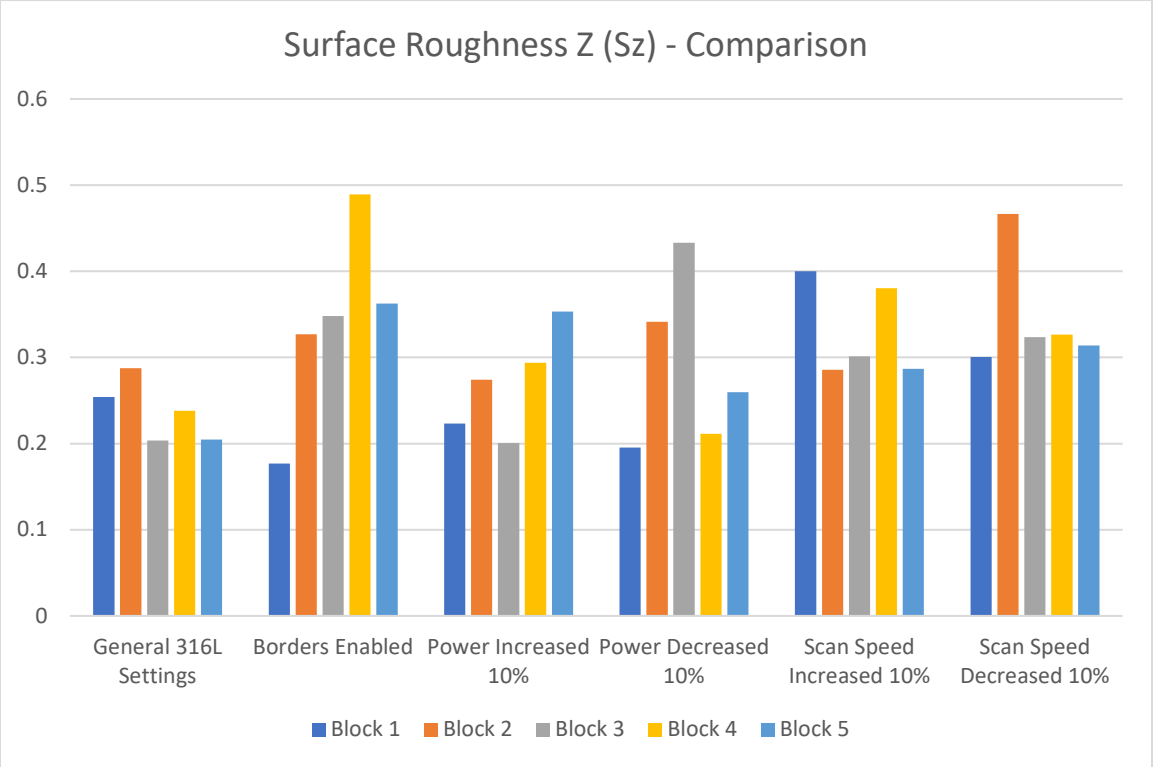

Figure 36: Sz Comparison

Figures 37 and 38 below show the artifact surfaces at 500x. Figure 37 is the artifact printed under “Parameter Set 1 – General 316L Settings” and Figure 38 is the artifact printed under “Parameter Set 2 – Borders Enabled”.

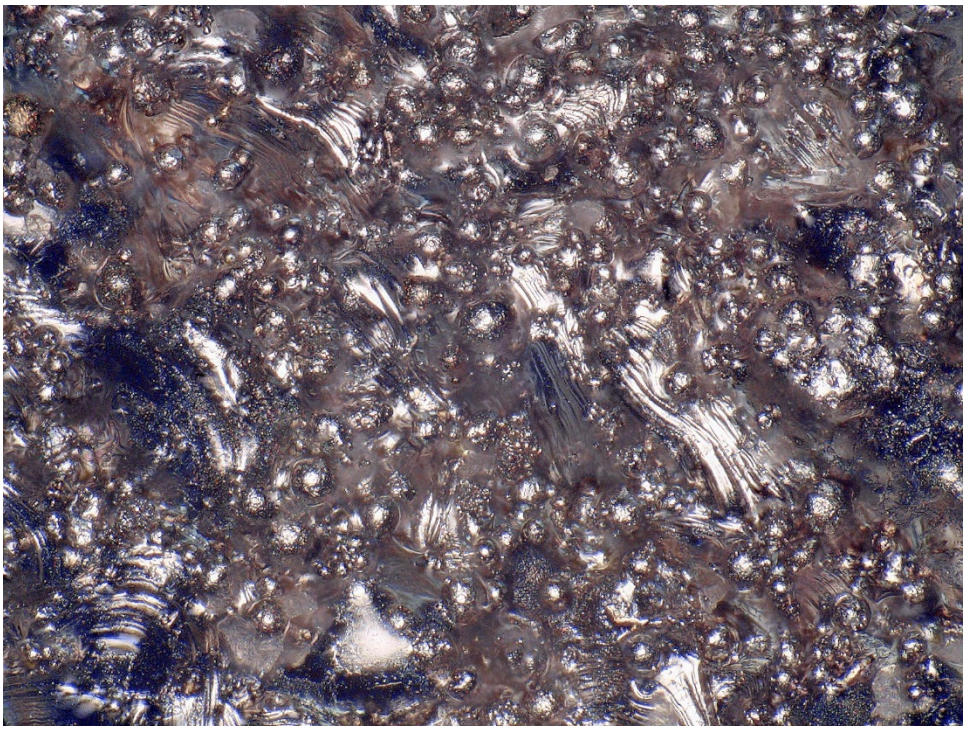

Figure 37: Parameter Set 1 Surface - 500x

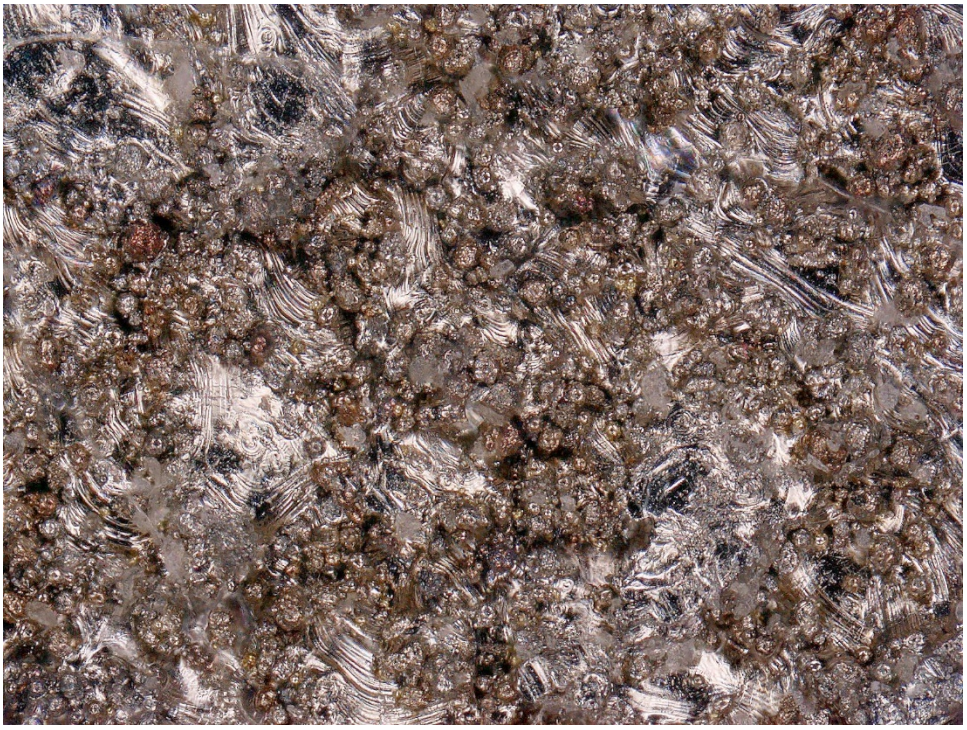

Figure 38: Parameter Set 2 Surface - 500x

Section 4.7 – XRF Results

The XRF analysis was done in three different locations across each of the five applicable parameter sets. As stated in Section 3.5, “Parameter Set 2 – Borders Enabled” was not studied because the surface was ground off, removing any potential effects of a surface process such as the border laser rescans. The goal of the XRF analysis was twofold; to show that minimal amount of contaminants were picked up during the printing process, and to show that the final composition remained alloyed Kovar and did not separate into its parts.

The results were consistent across all five parameter sets examined, showing that little to no contaminants were picked up during the printing process, and the Iron, Cobalt, and Nickel are remaining alloyed into Kovar steel. One of the analysis reports is shown below in Figure 39.

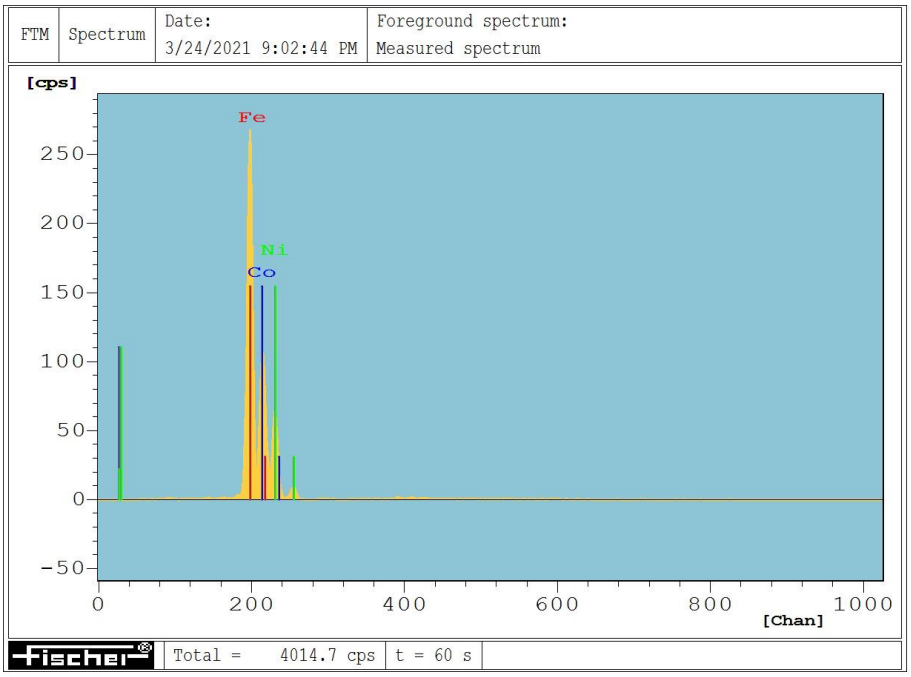

Figure 39: Parameter Set 6 XRF Results

Chapter 5 – Conclusion

Section 5.1 – Conclusion

Overall, this work fulfilled its original goals and laid the groundwork for future studies in additively manufactured Kovar steel. While throughout the study the scope changed, it provides successful parameters under which to produce parts with appropriate CTE and gives initial conclusions on what parameters should be further investigated. Initial CTE results are showing well within the range for Kovar steel as described in Table 1. Considering the applications of Kovar steel, CTE is likely the most important property to consider. If the CTE of the additively manufactured material was found to be significantly higher, it would not be a viable manufacturing approach.

A breakdown of the results under which conclusions will be made is shown in Table 5. Ultimate tensile strength, density, Charpy impact toughness, and roughness were all examined for the best performing parameter set. Performing best in all but one of those categories was "Parameter Set 1 – General 316L Settings", showing that the initial logic of basing the parameters on the laser welding guide was sound.

Parameter Set Performance by Property		
	Best Performing	Worst Performing
Ultimate Tensile Strength	General 316L Settings	Power Decreased 10%
Density	General 316L Settings	Scan Speed Increased 10%
Charpy Impact Toughness	Power Increased 10%	Scan Speed Decreased 10%
Roughness	General 316L Settings	Borders Enabled

Table 5: Parameter Set Performance by Property

The fact that “Parameter Set 3 - Laser Power Increased 10%” drastically over performed the other parameter sets in the Charpy testing and was close the performance of “Parameter Set 1 - General 316L Settings” shows that further parameter variation studies must be completed. If a parameter set combining the Charpy results of “Parameter Set 3 - Laser Power Increased 10%” and all of the results from “Parameter Set 1 - General 316L Settings” could be determined it would be a success for additively manufactured Kovar steel.

While “Parameter Set 1 – General 316L Settings” had a greater overall performance than the rest of the parameter sets, it still falls short of traditionally manufactured Kovar steel. Additively manufactured artifacts do not reach the same performance as traditionally manufactured materials but offer several advantages as seen throughout Chapter 1 of this Thesis.

Section 5.2 – Design Properties for Additively Manufactured Kovar Steel

The design properties shown in Table 6 below follow the performance of “Parameter Set 1 – General 316L” settings.

Design Properties for AM Kovar Steel per Parameter Set 1 – General 316L Settings	
Ultimate Tensile Strength	408.5 MPa
Density	7.71 g/cm^3
Charpy Impact Toughness	69.75 Joules
Rockwell Hardness C	51.9
Roughness; Ra, Rz, Sa, Sz	0.015, 0.099, 0.016, 0.24 mm

Table 6: AM Kovar Design Properties

Section 5.3 – Future Work

The study into additively manufactured Kovar steel will certainly continue from this initial study as it has implications for the needs of Sandia National Laboratories and will aid in setting a successful approach to new material characterization. Future efforts will certainly have much larger sample sizes to allow for more robust statistical analysis and parameters will be varied over greater ranges and at finer increments. More process parameters such as laser focus point, layer thickness, powder reuse, and support lattice effects will be studied. Tensile samples will likely be high-throughput samples, or alternatively the tests will be performed with an extensometer.

As this project moves forward it will be simple to complete these parameter set comparisons at finer increments as it is now possible to apply different parameter settings to different artifacts on the build plate. This will allow the number of parameter sets to not be the limiting factor on the build plate, but instead the number of artifacts that can fit on the plate. With this feature there will be no worry about reuse status of powder between different prints causing inconsistencies, because comparisons will be done with the printed test artifacts consisting of the exact same powder.

Future projects in additively manufactured Kovar steel include a residual stress study. The experimental design calls for instrumenting a Renishaw AM400 build plate with both strain gauges and thermocouples. To achieve this, a build plate has had portions machined out so that smaller, instrumented, plates can be inserted and printed upon. The goal is to collect the thermal and strain information throughout the build to make conclusions about the residual stress being produced in the part. The data will also be collected during the EDM

process. If this approach proves to be an accurate way to quantify the residual stress within a part, ways to potentially reduce that stress will be explored.

References

[1] Askeland, Donald R. (January 2015). "22-4 Thermal Shock". The Science and Engineering of Materials. Wright, Wendelin J. (Seventh ed.). Boston, MA. pp. 792–793. ISBN: 978-1-305-07676-1

[2] The Rise of Additive Manufacturing. (2016, May 6). Retrieved April 03, 2021, from https://simulatemore.mscsoftware.com/the-rise-of-additive-manufacturing/

[3] Koepke, Joshua Robert; Bradley Jared; and Yu-Lin Shen. "The Influence of Process Variables on Physical and Mechanical Properties in Laser Powder Bed Fusion." (2019). https://digitalrepository.unm.edu/me_etds/164

[4] Duda, T., & Raghavan, L. (2016, December 22). 3D Metal Printing Technology. Retrieved April 03, 2021, from https://www.sciencedirect.com/science/article/pii/S2405896316325496

[5] MMPDS-13: Metallic Materials Properties Development and Standardization

[6] Patzer, W., Strikwerda, P., Trimble, H., Exaddon, E., & Tutor, J. (2020, December 14). Metal 3d printing: An overview of the most common types. Retrieved April 03, 2021, from https://3dprinting.com/metal/types-of-metal-3d-printing/

[7] Leung, C., Marussi, S., Towrie, M., Atwood, R., Withers, P., & Lee, P. (2018, December 14). The Effect of Powder Oxidation on Defect Formation in Laser Additive Manufacturing. Retrieved April 03, 2021, from https://www.sciencedirect.com/science/article/pii/S1359645418309698

[8] Donaldson, B. (2018, April 23). What effect Does gas flow have in Metal Additive Manufacturing? Retrieved April 03, 2021, from https://www.additivemanufacturing.media/articles/what-effect-does-gas-flow-have-in-metal-additive-manufacturing

[9] Huckstepp, A. (2019, June 17). Powder Bed Fusion. Retrieved April 03, 2021, from https://www.digitalalloys.com/blog/powder-bed-fusion/

[10] Narayan, R. (2020). Rapid prototyping of biomaterials: Techniques in additive manufacturing. In *Rapid prototyping of biomaterials: Techniques in additive manufacturing* (pp. 17-40). Duxford: Elsevier/Woodhead Publishing.

[11] Hughes, S. E. (2009). Non-Destructive and Destructive Testing. In *A quick guide to welding and weld inspection* (pp. 67-87). New York: ASME Press.

[12] S.H. Baghjari, S.A.A. AkbariMousavi (2014). Experimental Investigation on Dissimilar Pulsed Nd:YAG Laser Welding of AISI 420 Stainless Steel to Kovar Alloy

[13] Surface Roughness Parameters. (n.d.). Retrieved April 03, 2021, from https://www.keyence.com/ss/products/microscope/roughness/line/parameters.jsp

[14] Whitehouse, David (2012). Surfaces and their Measurement. Boston: Butterworth-Heinemann. ISBN 978-0080972015.

[15] Schuetz, G. (2002, November 01). Surface Texture from Ra to Rz. Retrieved April 03, 2021, from https://www.mmsonline.com/columns/surface-texture-from-ra-to-rz

[16] Zhai, C.; Gan, Y.; Hanaor, D.; Proust, G.; Retraint, D. (2016). "The Role of Surface Structure in Normal Contact Stiffness". Experimental Mechanics. **56** (3): 359–368. doi:10.1007/s11340-015-0107-0

[17] Stackpole, B. (2017, November 28). Materialise Takes the Pain Out of Support Generation for Metal 3D Printing. Retrieved April 03, 2021, from https://www.digitalengineering247.com/article/materialise-takes-the-pain-out-of-support-generation-for-metal-3d-printing

[18] Dutrow, B. L., & Clark, C. M. (2020, February 14). X-ray Powder Diffraction (XRD). Retrieved April 03, 2021, from https://serc.carleton.edu/research_education/geochemsheets/techniques/XRD.html

SNL is managed and operated by NTESS under DOE NNSA contract DE-NA0003525